A new modification of nickel selenite $NiSeO_3$—crystal structure and magnetic properties

2007 J. Phys.: Condens. Matter 19 196203

(http://iopscience.iop.org/0953-8984/19/19/196203)

IOP PUBLISHING JOURNAL OF PHYSICS: CONDENSED MATTER

J. Phys.: Condens. Matter **19** (2007) 196203 (14pp) doi:10.1088/0953-8984/19/19/196203

A new modification of nickel selenite $NiSeO_3$—crystal structure and magnetic properties

M Miljak[1], R Becker[2], M Herak[1], M Prester[1], O Milat[1], M Johnsson[2] and H Berger[3]

[1] Institute of Physics, POB 304, HR-10 000, Zagreb, Croatia
[2] Department of Inorganic Chemistry, Stockholm University, S-106 91 Stockholm, Sweden
[3] Institute de Physique de la Matière Complexe, EPFL, CH-1015 Lausanne, Switzerland

E-mail: miljak@ifs.hr and richard@inorg.su.se

Received 6 November 2006, in final form 31 January 2007
Published 18 April 2007
Online at stacks.iop.org/JPhysCM/19/196203

Abstract

The crystal structure of a new modification of $NiSeO_3$ is described together with its magnetic properties. The new polymorph crystallizes in the monoclinic system, space group $C2/c$, with unit cell parameters $a = 15.4965(7)$ Å, $b = 9.8250(4)$ Å, $c = 14.7278(8)$ Å, $\beta = 110.610(4)^\circ$ and $Z = 8$. The crystal structure was solved from single crystal data, $R = 0.0252$. The structure can be considered as being layered along the bc-plane with $[NiO_6]$ octahedra arranged into two sub-groups. The layers are further connected to adjacent layers via groups of two edge-sharing $[NiO_6]$ octahedra. The Ni octahedra are tilted and are either edge or corner sharing, giving rise to two different Ni–Ni interactions. The lone pairs of Se^{4+} occupy non-bonding regions of tunnels along [001] and [010]. The complexity of the crystal structure is also reflected in the complex low-temperature magnetic state. An antiferromagnetic-like transition was observed at $T_{tr} = 14.4$ K. A possible structural rearrangement closely above T_{tr} complicates the details of the low-temperature state. The antiferromagnetic-like transition disagrees with the features of a three-dimensional (3D) Néel antiferromagnetic ordering. This is mostly because of the fact that the assumed bulk easy-axis susceptibility at the lowest temperature remains at high paramagnetic value. The consequences of the complex structure on basic magnetic parameters, zero-field splitting energy D and exchange coupling J, and accordingly on the magnetic properties, are discussed.

(Some figures in this article are in colour only in the electronic version)

1. Introduction

Compounds containing main group elements that have a stereochemically active lone pair, e.g. Te^{4+}, Se^{4+}, and Sb^{3+}, show a rich structural chemistry, partly due to the asymmetric coordination around those cations. The lone electron pair will often function as 'chemical scissors' to effectively open up the crystal structure and give rise to layered or hollow compounds [1–7]. $NiSeO_3$ has previously been known to crystallize in the orthorhombic space group $Pnma$ [8]. This study reports the crystal structure and the magnetic properties of a new monoclinic ($C2/c$) modification of $NiSeO_3$. Several other transition metal selenites with the general formula $M^{2+}SeO_3$ have been described (M = Mg, Mn, Co, Cu, Zn) and all these crystallize in the orthorhombic space group $Pnma$ [8]. $CoSeO_3$ also exists in a monoclinic ($C2/c$) modification that is iso-structural with the title compound [9]. Due to Jahn–Teller distortion, $CuSeO_3$ has been found in three modifications in addition to the orthorhombic ($Pnma$): an orthorhombic ($Pcab$), a monoclinic ($P2_1/n$), and a triclinic ($P\bar{1}$) [10]. Some hydrated nickel selenites have also been reported: the monoclinic ($P2_1/n$) mineral Ahlfeldite $NiSeO_3{\cdot}2H_2O$ [11] and triclinic ($P\bar{1}$)$Ni_3(SeO_3)_3{\cdot}H_2O$ [12, 13].

The magnetic properties of the nickel(II) (Ni^{2+} ion) compounds have been studied extensively both experimentally and theoretically since the 1950s [14]. Owing to the integer spin $S = 1$, Haldane's conjecture about the difference between antiferromagnetic Heisenberg chains with integer and non-integer spins [15] renewed much interest in the nickel(II) magnetic systems. A diversity of magnetic behaviour in the nickel(II) magnetic systems seems to be due, as has been discussed [16], to the virtually random affinity of the nickel(II) for both signs of the zero-field splitting energy D. Thus, depending on the interrelation between the two relevant magnetic quantities imposed by the crystal structure (the zero-field splitting energy D and the exchange coupling J between nickel(II) moments), a variety of low-temperature magnetic states may result. The magnetic properties of the orthorhombic modification of $NiSeO_3$ [8] seem to be fully governed by moderate antiferromagnetic coupling between nickel (II) magnetic moments realized via corner-sharing connection of the NiO_6 octahedra. In other words, observations of a moderate Curie–Weiss temperature, $\Theta = -256$ K, and a sizable antiferromagnetic transition temperature of $T_N = 96$ K [8] are compatible with Heisenberg-exchange-driven ordering of $S = 1$ spins.

This magnetic study of a new monoclinic modification of $NiSeO_3$ appears not to be so conclusive, as one could anticipate from the much more complex crystal structure compared to the former orthorhombic modification. It is the presence of an additional way of connecting NiO_6 octahedra in this structure (the edge-sharing connection between NiO_6 octahedra) which accordingly generates an additional exchange path, but of different type to that in the case of corner sharing. Thus, the presence of both types of connection generates type-exchange frustration on the nickel(II) site, with consequences for the low-temperature magnetic state.

2. Experimental details

2.1. Synthesis

The new compound $NiSeO_3$ was synthesized via chemical vapour transport reaction. The starting materials were: NiO (Alfa Aesar 99.998%), SeO_2 (Alfa Aesar 99.4%) and $NiBr_2$ (Aldrich 99.99 + %). The large single crystals used in this study were grown from mixtures of NiO, SeO_2 and $NiBr_2$ in the off-stoichiometric molar ratio 4:8:2, respectively.

The transport reaction was performed in closed silica ampoules ($l = 250$ mm, $d = 20$ mm). To reduce the water content to a reproducible amount, the ampoules were heated for

10 h at $T = 1000\,^{\circ}$C under a vacuum of 10^{-5} Torr before they were filled and sealed off. The non-stoichiometric starting mixture was included at one side, and then the tube was evacuated to 10^{-5} Torr, at which time HBr electronic-grade gas was introduced at room temperature into this tube, which was subsequently sealed off. One end of the tube (with the reactants) was heated for 24 h, while the other end was left outside the furnace. A mixture of SeO_2 and $NiBr_2$ condensed at the cold end of the tube. As the tube was then gradually moved into the furnace, a large quantity of the mixture reacted. The temperatures at the ends of the tube were at 750 and 700 °C. After two weeks, the formation of two types of single crystals was observed:

(i) bright yellow plates of monoclinic $NiSeO_3$ with a maximum size of $4 \times 2 \times 0.5$ mm^3; and
(ii) some plates of orange $Ni_5(SeO_3)_4Br_2$ crystals [17] with a maximum size of $6 \times 3 \times 0.2$ mm^3. Also, an uncharacterized yellow-orange crystalline powder was present.

The synthesis products were characterized in a scanning electron microscope (SEM, JEOL 820) with an energy-dispersive spectrometer (EDS, LINK AN10000), confirming the presence and stoichiometry of Ni and Se and the absence of Br.

2.2. Crystal structure determination

Single-crystal x-ray data were collected with an Oxford Diffraction Xcalibur3 diffractometer using graphite-monochromatized Mo Kα radiation ($\lambda = 0.710\,73$ Å). The intensities of the reflections were integrated and Gaussian absorption correction was made using the software supplied by the manufacturer [18]. The crystal structures were solved by direct methods using the program SHELXS97 [19] and refined by full matrix least squares on F^2 using the program SHELXL97 [20]. All atoms were refined using anisotropic displacement parameters. Experimental parameters for the monoclinic form of $NiSeO_3$ are reported in table 1.

2.3. Magnetic measurements

Static (dc) susceptibility measurements of the powdered sample were made using the Faraday method in a magnetic field up to 9 kOe and in the temperature range 2–330 K. The single-crystal susceptibility anisotropy $\Delta\chi = (\chi_x - \chi_y)$, where x and y denote magnetic axes, was obtained using a highly sensitive torque magnetometer in the temperature range 2–330 K in fields of up to 8 kOe. A low-field (ac) susceptibility (1 Oe typically, at the measuring field frequency of 430 Hz) was measured on the single crystal below 160 K by the use of a commercial CryoBIND system.

3. Results

3.1. Crystal structure

The new $NiSeO_3$ polymorph crystallizes in the monoclinic system, space group $C2/c$. Experimental parameters, atomic coordinates and selected interatomic distances and angles are reported in tables 1–3, respectively. The title compound is iso-structural with $CoSeO_3$-II [9].

The structure consists of a three-dimensional network that contains intersecting channels, however it can be regarded as being layered in the bc-plane; see figures 1–3. There are four crystallographically different Se^{4+} positions and four different Ni^{2+} positions, all having the Wyckoff position 8f. All four Se^{4+} cations have the classical tetrahedral [SeO_3E] coordination, where E designates the $4s^2$ lone-pair electrons on Se^{4+}, with Se–O distances ranging from 1.675(2) to 1.797(3) Å, and there is no fourth oxygen present closer than ∼2.7Å. The positions of E have been calculated using Se–E distances of 1.21 Å according to Galy *et al* [21]; see

Table 1. Crystal data for monoclinic $NiSeO_3$.

Empirical formula	$NiSeO_3$
Formula weight	742.68
Temperature	292(3) K
Wavelength	0.71073 Å
Crystal system	Monoclinic
Space group	$C2/c$
Unit cell dimensions	$a = 15.4965(7)$Å
	$b = 9.8250(4)$ Å
	$c = 14.7278(8)$ Å
	$\beta = 110.610(4)^\circ$
Volume	2098.84(17) Å^3
Z	8
Density (calculated)	4.701 g cm^{-3}
Absorption coefficient	21.006 mm^{-1}
Absorption correction	Gaussian
F(000)	2752
Crystal colour	Yellow
Crystal habit	Thin flake
Crystal size (mm)	$0.120 \times 0.080 \times 0.040$ mm^3
θ range for data collection	4.23°–28.93°
Index ranges	$-21 \leqslant h \leqslant 21$
	$-13 \leqslant k \leqslant 13$
	$-20 \leqslant l \leqslant 8$
Reflections collected	7916
Independent reflections	2745 [R(int) = 0.0561]
Completeness to $\theta = 28.93^\circ$	98.0%
Refinement method	Full-matrix least squares on F^2
Data/restraints/parameters	2745/0/182
Goodness-of-fit on F^2	1.075
Final R indices [$I > 2\theta(I)$]	$R1 = 0.0252$
	$wR2 = 0.0620$
R indices (all data)	$R1 = 0.0284$
	$wR2 = 0.0635$
Largest diff. peak and hole	1.237 and -0.867 e Å^{-3}

table 4. All four Ni^{2+} cations have distorted octahedral [NiO_6] coordinations and are tilted with respect to the crystal axes. The Ni–O distances are in the range 2.009(2)–2.234(2) Å. Bond valence sum calculations according to Brown [22] confirm the oxidation states of all ions; see table 2.

The layers along the *bc*-plane are made up of the [Ni(2)O_6], [Ni(3)O_6], and [Ni(4)O_6] octahedra. These are arranged to form two different building units: edge-sharing Ni(4)–Ni(2)–Ni(2)–Ni(4) octahedra forming a {Ni_4O_{18}} group, and pairs of two edge-sharing Ni(3) octahedra forming a {$Ni(3)_2O_{10}$} unit. Different {Ni_4O_{18}} groups run along [011] as well as [$0\bar{1}1$]. Each such unit is connected via corner sharing to four other units of the same kind and to four {$Ni(3)_2O_{10}$} groups; see figure 3. The edge and corner sharing gives rise to two different Ni–Ni couplings, which result in the two possible J interactions discussed in the magnetic section.

The layers are connected by groups of two edge-sharing [Ni(1)O_6] octahedra, forming a {$Ni(1)_2O_{10}$} group, via edge and corner sharing to the Ni octahedra within the layers. All the

Table 2. Atomic coordinates and equivalent isotropic displacement parameters for monoclinic $NiSeO_3$. All atoms have the Wyckoff position 8f.

Atom	x	y	z	U_{eq}[a] (Å^2)	BVS[b]
Se(1)	0.376 95(2)	0.133 35(4)	0.103 38(2)	0.0091(1)	3.82
Se(2)	0.084 71(2)	0.116 04(3)	0.363 91(2)	0.0077(1)	4.00
Se(3)	0.386 15(2)	0.318 18(4)	0.351 40(2)	0.0086(1)	3.78
Se(4)	0.094 77(2)	0.381 80(3)	0.180 71(2)	0.0082(1)	4.13
Ni(1)	0.069 20(3)	0.115 61(4)	0.034 01(3)	0.0080(1)	2.02
Ni(2)	0.260 03(3)	0.364 91(5)	0.090 01(3)	0.0095(1)	1.95
Ni(3)	0.233 22(3)	0.355 95(5)	0.416 63(3)	0.0087(1)	2.07
Ni(4)	0.224 63(3)	0.092 41(5)	0.241 71(3)	0.0086(1)	1.90
O(1)	0.343 0(2)	0.266 7(3)	0.018 8(2)	0.0091(5)	1.94
O(2)	0.311 4(2)	0.015 6(3)	0.024 3(2)	0.0120(5)	2.10
O(3)	0.309 0(2)	0.185 4(3)	0.166 6(2)	0.0120(5)	1.88
O(4)	0.168 4(2)	0.196 2(3)	0.454 5(2)	0.0113(5)	2.11
O(5)	0.030 5(2)	0.013 4(3)	0.420 9(2)	0.0099(5)	2.00
O(6)	0.146 5(2)	0.000 0(3)	0.324 9(2)	0.0106(5)	1.91
O(7)	0.465 2(2)	0.261 1(3)	0.454 3(2)	0.0121(5)	1.82
O(8)	0.290 6(2)	0.226 0(3)	0.346 6(2)	0.0101(5)	2.07
O(9)	0.337 4(2)	0.470 2(3)	0.381 2(2)	0.0094(5)	1.92
O(10)	0.113 45(2)	0.396 5(3)	0.299 8(2)	0.0117(5)	1.76
O(11)	0.112 1(2)	0.212 8(3)	0.165 9(2)	0.0104(5)	2.01
O(12)	0.195 6(2)	0.441 6(3)	0.176 5(2)	0.0128(5)	2.15

[a] U_{eq} is defined as one third of the trace of the orthogonalized U tensor.
[b] Constants for the bond valence sum (BVS) calculations are from [22, 23].

Table 3. Selected bond lengths (Å) for monoclinic $NiSeO_3$. Note, symmetry codes: (i) $-0.5 + x$, $0.5 - y$, $-0.5 + z$; (ii) x, $-y$, $-0.5 + z$; (iii) $0.5 - x$, $0.5 - y$, $-z$; (iv) $0.5 - x$, $-0.5 + y$, $0.5 - z$; (v) $-x$, y, $0.5 - z$; (vi) $0.5 - x$, $0.5 + y$, $0.5 - z$; (vii) $0.5 - x$, $0.5 - y$, $1 - z$.

Se(1)–O(1)	1.756(2)	Ni(2)–O(1)	2.152(2)
Se(1)–O(2)	1.701(2)	Ni(2)–O(12)	2.020(2)
Se(1)–O(3)	1.711(2)	Ni(2)–O(1)^{iii}	2.234(2)
Se(2)–O(4)	1.692(2)	Ni(2)–O(2)^{iii}	2.031(2)
Se(2)–O(5)	1.710(2)	Ni(2)–O(3)	2.086(3)
Se(2)–O(6)	1.713(2)	Ni(2)–O(6)^{vi}	2.038(2)
Se(3)–O(7)	1.675(2)	Ni(3)–O(10)	2.077(3)
Se(3)–O(8)	1.716(2)	Ni(3)–O(2)^{vi}	2.030(3)
Se(3)–O(9)	1.797(3)	Ni(3)–O(4)	2.045(3)
Se(4)–O(10)	1.680(2)	Ni(3)–O(4)^{vii}	2.038(3)
Se(4)–O(11)	1.708(3)	Ni(3)–O(8)	2.033(2)
Se(4)–O(12)	1.691(2)	Ni(3)–O(9)	2.175(3)
Ni(1)–O(11)	2.054(2)	Ni(4)–O(11)	2.077(3)
Ni(1)–O(1)^{iii}	2.130(2)	Ni(4)–O(12)^{iv}	2.032(3)
Ni(1)–O(5)^{ii}	2.009(2)	Ni(4)–O(3)	2.188(2)
Ni(1)–O(5)^{v}	2.135(2)	Ni(4)–O(6)	2.199(2)
Ni(1)–O(7)^{i}	2.028(3)	Ni(4)–O(8)	2.010(2)
Ni(1)–O(9)^{iv}	2.103(2)	Ni(4)–O(9)^{iv}	2.102(2)

$[NiO_6]$ octahedra are connected via corner and edge sharing to the $[SeO_3E]$ tetrahedra, so that the lone pairs on Se^{4+} protrude into non-bonding regions in between the layers, resulting in channels in the crystal structure; see figures 1 and 2.

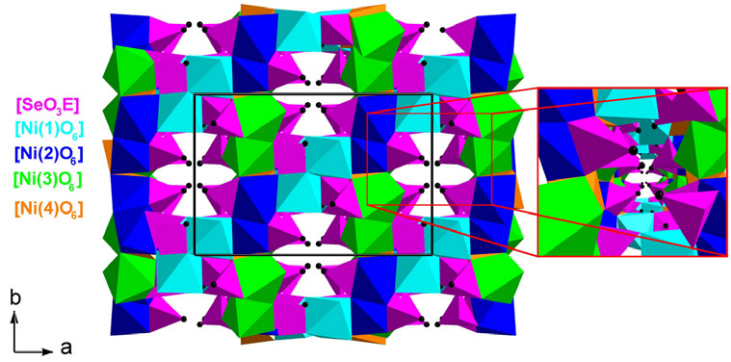

Figure 1. The crystal structure of monoclinic $NiSeO_3$ seen along [001]. The inset shows a projection view of a non-bonding region 'occupied' by lone pairs E (black spheres).

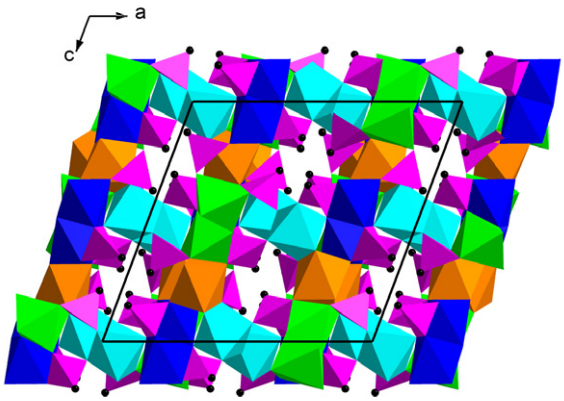

Figure 2. Monoclinic $NiSeO_3$ seen along [010]; same labelling as in figure 1.

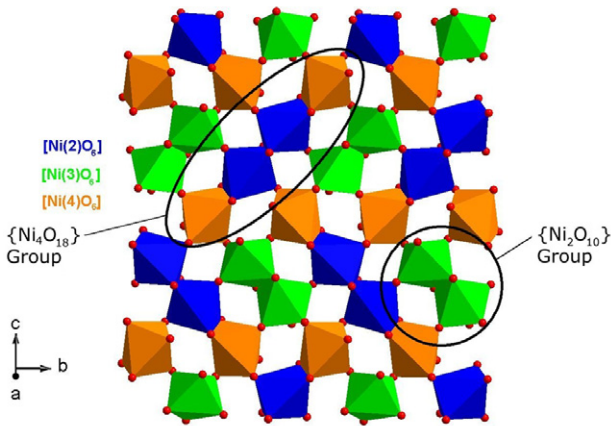

Figure 3. A single layer of Ni–octahedra stretching along the *bc*-plane where the two different edge-sharing building units $\{Ni_4O_{18}\}$ and $\{Ni_2O_{10}\}$ have been marked; oxygen (spheres).

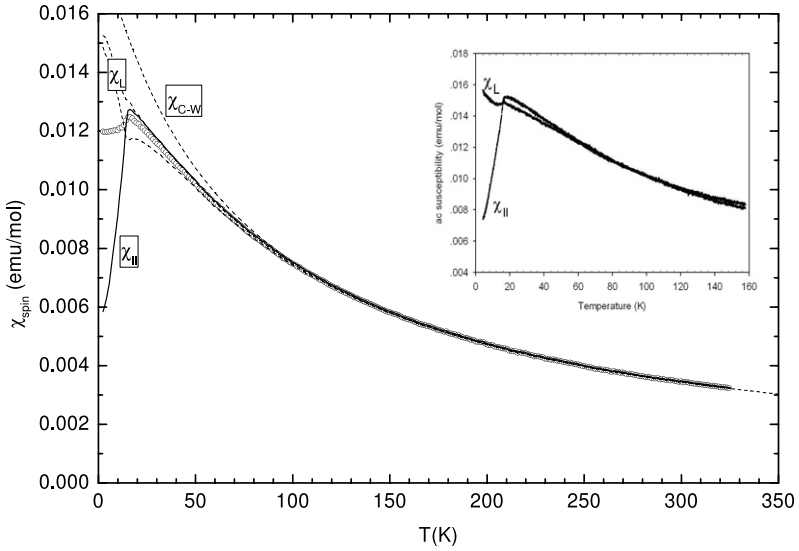

Figure 4. Temperature dependence of the dc powder spin susceptibility—closed circle. Inset: temperature dependence of the ac susceptibilities for the two mutually perpendicular sample orientations. The three bulk dc susceptibilities: $\chi_{\parallel}$—solid line, $\chi_{\perp}$—dashed lines. High-temperature Curie–Weiss susceptibility, $\chi_{\mathrm{CW}} = 1.267/(T + 68)$—dotted line.

Table 4. Coordinates for the calculated E positions.

Cation	*X*	*Y*	*Z*
Se(1)	0.455 45	0.101 61	0.150 47
Se(2)	0.034 42	0.192 43	0.304 06
Se(3)	0.418 63	0.316 84	0.287 76
Se(4)	0.023 05	0.431 34	0.128 28

The compound $Ni_3(SeO_3)_3{\cdot}H_2O$ [12, 13] has a crystal structure related to the title compound with non-bonding regions or channels in between the layers where the lone pairs are located, but the layers in $Ni_3(SeO_3)_3{\cdot}H_2O$ are positioned closer to each other with a single $[NiO_6]$ octahedron connecting them instead of the $\{Ni_2O_{10}\}$ group, which is the case in the title compound.

3.2. Magnetic properties

3.2.1. Magnetic susceptibility and torque magnetometry. Magnetic susceptibility of $NiSeO_3$ samples in the form of single crystals and powder has been measured by the use of ac and dc susceptibility, respectively. Figure 4 displays the static susceptibility measurements of the powdered single crystal, while the inset presents ac susceptibility data. In $NiSeO_3$, nickel is in the Ni^{2+} ionic state and one expects magnetic features compatible with the $S = 1$ spin state. Indeed, from the high-temperature Curie–Weiss behaviour, figure 4 (dashed line), we obtain a Curie constant of $C = 1.267$ and the corresponding average g-factor value of $\langle g \rangle = 2.26$ ($\mu_{\mathrm{eff}} = 3.19\ \mu_{\mathrm{B}}$), similar to what is frequently reported for the Ni^{2+} ion. In obtaining the spin susceptibility, the only correction made to the raw data consists of referencing them to the sum of temperature-independent diamagnetism, -1.2×10^{-4} emu mol^{-1} [24], and a temperature-independent orbital contribution of $+3 \times 10^{-4}$ emu mol^{-1} for Ni^{2+} [25]. (In

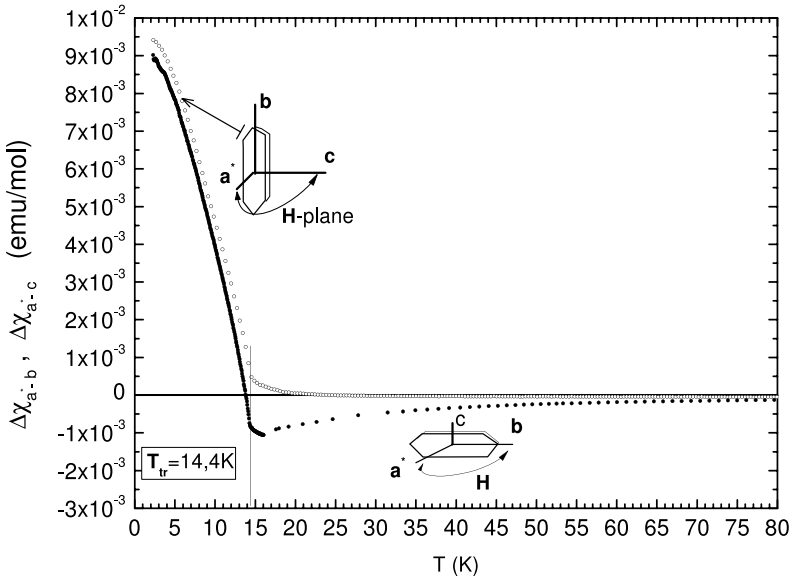

Figure 5. Temperature dependence of the anisotropy in the two different planes; (a^*–c)—open circles, and (a^*–b)—closed circles. Note the same resolution of the anisotropy axis as the susceptibility in figure 4. Note, also, the sketch of the sample morphology and the crystal axes positions, according to the x-ray check.

accordance with the interpretation of our results presented below, we note that the values obtained for the g-factor and Θ_{CW} are regarded as effective values.) Low-field (1 Oe) ac susceptibilities for the two sample orientations (applied field parallel or orthogonal to the sample plane) are shown in the inset of figure 4. Note the slight difference between dc and ac measurements of the temperature dependence of the bulk susceptibilities at temperatures below 15 K in figure 4 which, according to the independently determined crystal axes positions, is a consequence of the sample misorientation in the ac susceptibility measurements rather than sample-dependent effects. We found no other differences in the temperature dependence of the bulk susceptibilities obtained by ac and dc methods.

Single-crystal susceptibility anisotropies for the two mutually perpendicular sample orientations are presented in figure 5. In order to compare the directions of the magnetic axes with respect to the crystal axes, the orientations of the crystal axes were determined by an independent x-ray check. It turned out that only the c axis coincided with one of the bulk magnetic axes. Besides, the same x-ray data were free from crystal twinning effects. The sample morphology and the crystal axes, as obtained by the x-ray check, are sketched in figure 5.

The data of the static powder susceptibility, ac susceptibility and torque magnetometer are reminiscent of an antiferromagnetic transition below 15 K. However, the transition cannot be attributed to a three-dimensional antiferromagnetic Néel ordering for the following reasons.

Firstly, we note that the powder spin susceptibility above about 80 K follows Curie–Weiss behaviour with a negative Curie–Weiss temperature of $\Theta_{\mathrm{CW}} = -68$ K, signifying antiferromagnetic coupling. At about 15 K there is a cusp-like anomaly that is otherwise characteristic for antiferromagnetic orderings. Starting from its cusp value, the susceptibility decreases, by extrapolation to $T = 0$ K, by about 4% only: for a powdered sample in the case of standard Néel ordering, one would expect the relation $\langle\chi(0\ \mathrm{K})\rangle = 2/3\chi(T_{\mathrm{N}})$ to be satisfied instead.

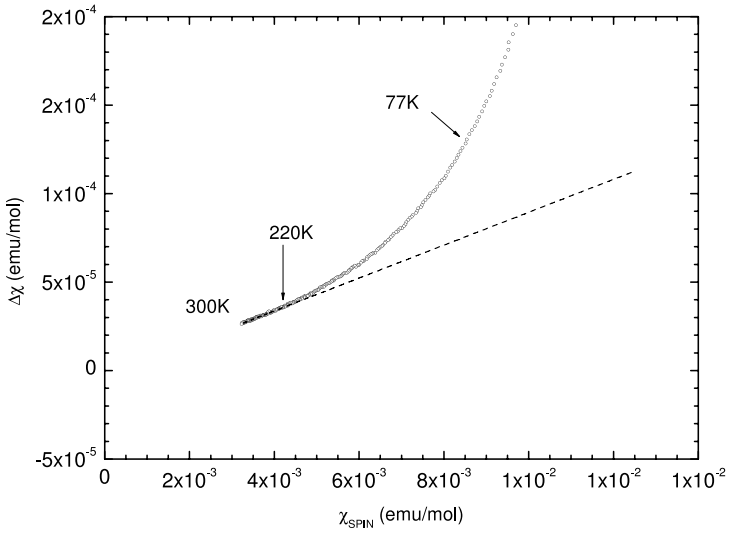

Figure 6. The correspondence between anisotropy in the (a^*–b) plane and the powder spin susceptibility.

Secondly, the torque measurements below temperature $T_{\mathrm{tr}} = 14.4$ K, for the two mutually perpendicular sample orientations, reveals the development of a large antiferromagnetic-like anisotropy, $\Delta\chi = (\chi_\perp - \chi_\parallel)$. However, the value of the anisotropy at the lowest temperatures appears to be reduced with respect to the three-dimensional antiferromagnetic Néel ordering ($\langle\Delta\chi(0\ \mathrm{K})\rangle = \chi(T_{\mathrm{N}})$).

Under the circumstances, one would first like to clarify whether the observed large value of the average susceptibility at $T = 0$ K, $\langle\chi(0\ \mathrm{K})\rangle$, is intrinsic or extrinsic in nature. In order to resolve this question, we present high-temperature data of the susceptibility and the anisotropy in a *correspondence diagram* ($\Delta\chi(T)$ versus $\langle\chi(T)\rangle$ data plot); see figure 6.

The diagram reveals a nonlinear correspondence between the powder spin susceptibility of the Curie–Weiss form and the measured anisotropy. The nonlinearity in this diagram indicates either an anisotropic contribution of the paramagnetic impurities (via g-factor anisotropy), differing in its temperature dependence from the Curie–Weiss form of the powder susceptibility, or the small anisotropy originating from the intrinsic single-ion anisotropy. On the lowest-temperature side, a diverging contribution to the susceptibility of the paramagnetic impurities would result in a non-saturating form of the temperature dependence of the measured anisotropy ($\chi_\perp - \chi_\parallel$) below 4.2 K. The measured form of susceptibility anisotropy was found to be of the saturating type, thus discarding the mono-ionic paramagnetic impurities as a cause of the nonlinear correspondence curve. We remark here that the saturating feature of the measured anisotropy at the lowest temperatures can result not only from the temperature dependence of $\chi_\parallel$ in the case of antiferromagnetic ordering but also in the case of similarly large anisotropy originating from single-ion anisotropy, hence the feature cannot be used as a proof of antiferromagnetic ordering. Also, it is important to stress that a linear field dependence of magnetization was observed in the whole temperature range in both types of dc measurements: the susceptibility and the torque (e.g. evidenced by the 180° periodicity of the regular torque curves; inset of figure 7). Thus, a large value of the powder susceptibility at 2 K and a reduced value of the anisotropy ($\chi_\perp - \chi_\parallel$) at 2 K are attributed to the intrinsic bulk quantities.

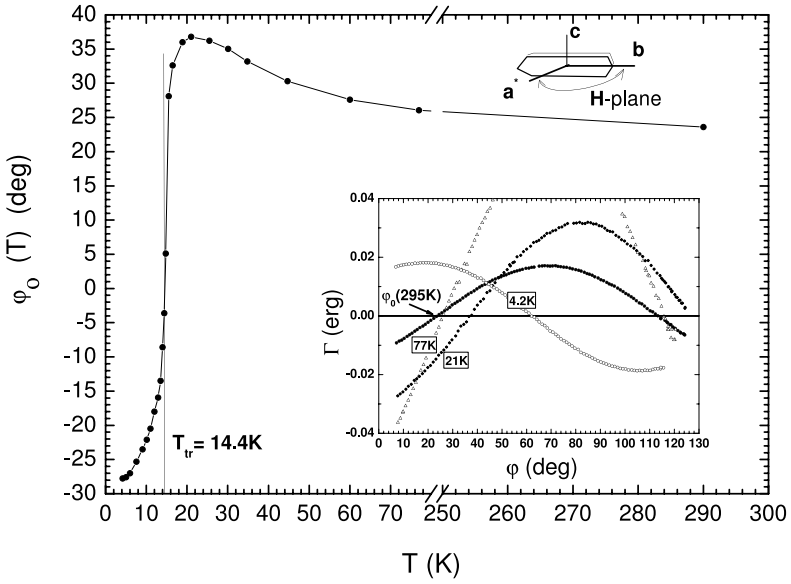

Figure 7. Temperature dependence of the zero crossing point ϕ_0 of the torque curve. Inset: the torque curves at a few fixed temperatures. The torque curves at 295 K and 77 K are obtained in a field of $H = 6$ kOe at 21 K in $H = 2.25$ kOe and at 4.2 K in a field of $H = 0.5$ kOe.

3.2.2. The nature of the transition at T_{tr}. In this section we elaborate more closely the problem of the nature of the antiferromagnetic-like transition at T_{tr}. As mentioned above, our experimental findings cast some doubts about the antiferromagnetically long-range-ordered ground state, especially in its standard Néel-type form. We show below that, apart from a feasible ground for ordering (weakly anisotropic exchange interaction) which can account for a low transition temperature, there is still a possibility of an alternative interpretation of the feature at $T_{tr} = 14.4$ K, in particular a combined effect of a sharp structural transition and the development of large paramagnetic anisotropy originating from the single-ion anisotropy.

Taking into account the combined data of the powder susceptibility and the two anisotropies, we extracted all three bulk dc susceptibilities, as displayed in figure 4. Assuming antiferromagnetic order below $T_{tr} = 14.4$ K, it appears that the susceptibility $\chi_{\|}$ is aligned close to the a^* axis, ending up at the lowest temperature at a large finite value (about an order of magnitude larger than the temperature-independent orbital contribution or the residual paramagnetism in antiferromagnets [26]). Such a large value of $\chi_{\|}$ at 2 K would offer a simple interpretation, i.e. that a third of the crystal remains in the paramagnetic (Curie–Weiss) phase down to 2 K, however the torque-magnetometer studies shown below indicate that some structural rearrangements may precede the magnetic transition, offering an alternative interpretation; see figure 7.

Figure 7 displays temperature dependence of the zero crossing point ϕ_0 of the regular torque curves (equation (1)), indicated by an arrow for $T = 295$ K in the inset, where m, ϕ and H denote the sample mass, magnetic field angle and magnetic field, respectively:

$$\Gamma(H) = \frac{m}{2M_{\text{mol}}} \sin[2(\phi - \phi_0)]H^2. \tag{1}$$

It is important to note here that the temperature dependence of the zero crossing point ϕ_0 present in the whole temperature range was observed only in the (a^*–b) plane. In going

from high to low temperatures, the ϕ_0 exhibits progressive displacement down to about 80 K, whereas above T_{tr} at 15 K it displays a rapid change of about 8° within 1 K, reminiscent of the structural transition. Similarly, sharp changes in ϕ_0 at an appropriate temperature in one of the organic chain compounds has been monitored in detail [27] where the structural transition was observed independently by x-ray measurements, while in the other compound the continuous type of temperature dependence of ϕ_0 below the temperature of nonmagnetic (dielectric) ordering was observed. The temperature dependence of the zero crossing point ϕ_0 is usually a consequence of the presence of the two anisotropic subsystems with different temperature-dependent magnetizations whose principal magnetic axes do not coincide. Actually, detailed measurements of $\Gamma(T)$, and accordingly of $\phi_0(T)$, are indeed compatible with the presence of the two sets of magnetic axes in the (a^*–b) plane making an angle of about 26°. Thus, continuous displacement of ϕ_0 from 295 K down to 80 K is a result of a superposition of the two sets of magnetic axes rather than a single set that exhibits continuous axes rotations caused by structural rearrangements from the highest temperatures already, because a nickel (II) ion, in contrast to Cu(II), is not regarded as a Jahn–Teller ion. Note also that the stronger temperature dependence of the zero crossing point ϕ_0 coincides with the deviation of the Curie–Weiss behaviour below 80 K shown in figure 4, thus signifying the intrinsic origin of both features. Considering the range of reported zero-field splitting energies D for nickel(II), the temperature of 80 K where deviation from the Curie–Weiss behaviour sets in appears to be too high, and can only be reconciled via subtle changes in the exchange coupling governed by the structure. Actually, an increase of only 8% in the exchange coupling below 80 K removes deviation of the Curie–Weiss behaviour down to about 25 K.

We tentatively ascribe the origin of structural rearrangement to a certain strongly distorted SeO_3 group [9] that shares oxygen with the appropriate NiO_6 octahedron and acts as a further linkage between structural units.

On one side, development of the short-range order above the supposed antiferromagnetic transition temperature $T_{tr} = 14.4$ K could contribute to the temperature dependence of ϕ_0. However, it cannot explain the whole temperature dependence of ϕ_0, which is present below the transition temperature and persists down to 4 K. The latter experimental fact, even if the transition at T_{tr} is antiferromagnetic, requires another subsystem of comparable large anisotropy in order to produce the temperature dependence of ϕ_0. Therefore, there is a possibility that the susceptibility behaviour in the transition range might be determined by structural features, coupled with large single-ion anisotropy, thus rendering the relevance of the exchange-driven ordering questionable. In the latter case, the effective Hamiltonian for spin $S = 1$ at site i in a magnetic field H (directed along the z-axis) takes the form of equation (2) [14], where J, D, E and g denote spin–spin exchange coupling, single-ion anisotropy (known also as a zero-field splitting energy), in-plane anisotropy and the electron g-factor, respectively:

$$\mathcal{H} = J\sum_i S_i \cdot S_{i+1} + D\sum_i (S_i^z)^2 + E\sum_i [(S_i^x)^2 - (S_i^y)^2] - \mu_B g H \sum_i S_i^z. \tag{2}$$

In the particular case of our monoclinic $NiSeO_3$ compound, with its magnetic properties reported herewith for the first time, no reliable data for the energies D and J are available. Therefore, we are unable to provide a quantitative argument favouring one over the other alternatives. Such an estimate would be inevitable in order to distinguish, for example, magnetic short-range order from the structural rearrangements as the mechanisms underlying the torque results. However, it is worth mentioning that the assumption of the presence of short-range order in a rather wide temperature range, from $T_{tr} = 14.4$ K up to 21 K, suggesting a two-dimensional nature of the underlying magnetism, is not in contradiction with the strong linear temperature dependence of the assumed perpendicular susceptibility below 14.4 K (figure 4).

3.2.3. Discussion of magnetic properties. Referring to the Hamiltonian equation (2) and our experimental results, one cannot ignore the possibility that the observed large susceptibility anisotropy at low temperatures actually relies on the weakly interacting [NiO_6] octahedra of sizable single-ion anisotropy D (such that $|J| \ll D$). Furthermore, the crystal structure of the compound reveals four different [NiO_6] octahedra interconnected by both corner and edge sharing. On the basis of the latter complexity, one could anticipate the possible presence of additionally contributing terms in equation (2). Firstly, because of the presence of the two Ni–Ni interacting paths, one expects at least two distinct spin–spin couplings J. Secondly, one also expects more than one distinct zero-field splitting energy D caused by different distortions of the four different [NiO_6] octahedra. Combining these two arguments, we may anticipate the spread of the zero-field splitting energies D and, accordingly, the spread of the ratio D/J. The latter distribution will certainly influence the circumstances of magnetic ordering [28, 29]. Even more, the presence of the edge-sharing connections could introduce anisotropic spin–spin exchange coupling, as is the case in a number of the [CuO_6]-based compounds with edge-sharing [CuO_6] octahedra. The presence of such an anisotropic exchange interaction introduces an Ising-type anisotropy and permits a magnetic ground state.

Summing up the subject of the involved magnetic interactions in monoclinic $NiSeO_3$, it seems very probable that the Hamiltonian equation (2) represents just a crude over-simplification. In this respect, it is very fruitful to discuss the magnetism/crystal structure relationship for the two $NiSeO_3$ modifications: the present monoclinic one and the previously reported [8] orthorhombic one. The susceptibility of orthorhombic $NiSeO_3$ follows Curie–Weiss behaviour with a Curie–Weiss temperature of $\Theta_{CW} = -250$ K, ordering antiferromagnetically at $T_N = 98$ K. The crystal structure reveals a three-dimensional network of corner-sharing [NiO_6] octahedra. Therefore, from the common relationship $\Theta_{CW} = (2\,z\,S\,(S+1)\,J)/(3\,k_B)$, where z represents six nearest neighbours, one can evaluate exchange coupling of $J/k_B \approx -32$ K. This value of J, combined with the frequently reported value for D of the Ni^{2+} ions of up to $D/k_B = 12$ K [29], implies $D/|J| < 1$, thus satisfying a condition for antiferromagnetic ordering. In addition, the presence of weak ferromagnetism below $T_N = 98$ K provides independent proof of the underlying antiferromagnetic order. Considering the experimental findings on orthorhombic $NiSeO_3$, one concludes that the ratio $D/|J| < 1$ is in basic accordance with the prediction of the antiferromagnetic ground state. However, one also concludes that the proposed simple Hamiltonian equation (2), which assumes a Heisenberg type of interaction, is less applicable; namely, the ratio T_N/Θ_{CW} in orthorhombic $NiSeO_3$ reaches a value of 0.4, while in the case of purely Heisenberg exchange-driven ordering of $S = 1$ spins [30] it is 0.72. It seems therefore that the Hamiltonian (2) is incomplete, missing some terms. For the present compound, assuming antiferromagnetic order, the ratio T_{tr}/Θ_{CW} is even smaller (0.2), pointing again to the drawbacks of (2).

We can estimate the value of J for monoclinic $NiSeO_3$ in the same way as we did for the orthorhombic counterpart. With the same coordination number $z = 6$ we get a value of J that is about three times smaller, $J/k_B = -8.8$ K. It turns out that the value of J that is obtained, though it represents the effective value, is comparable to or less than $D/k_B = 12$ K. The resulting ratio of $D/|J| \approx 1$ situates the present compound on the unstable borderline between the possible ground states.

In summary, it seems very likely that the distribution of the distinct values of D and of J, introduced by the four different [NiO_6] octahedra and at least the two different interacting paths, implies partial fulfillment of the conditions for magnetic ordering. As far as the low ordering temperature is concerned, this situation might have much in common with the theoretical study of NiF_2 [14]. In that study, three different exchange couplings J and a single D have been included in the Hamiltonian equivalent to equation (2). For the cases of D approaching J

(achieved by, for example, magnetic dilution), a rapid decrease in the Néel temperature, and hence a vanishing of antiferromagnetic order, has been shown to take place. The latter scenario could be relevant for the problems of questionable antiferromagnetism for monoclinic $NiSeO_3$. Regarding the crystal structure considerations, emphasizing layers of Ni octahedra in the (bc) plane, it might be the case that these are actually crystal objects differing from the rest of the crystal. Besides, the observed anisotropy above 80 K cannot result from a nearly isotropic g-factor of the Ni^{2+} moments of differently oriented [NiO_6] octahedra in the structure, but it can result from a macroscopic portion of the crystal with a suitable value of D. Finally, the presence of the structural rearrangements close above the transition temperature $T_{tr} = 14.4$ K allows an alternative possibility that the transition-like feature might be a result of superposition of the effects of a sharp structural transition (sharply changing crystal field parameters, and D, accordingly) and a large paramagnetic anisotropy associated with the nickel(II) single-ion anisotropy.

Further low-temperature investigations of the crystal structure, high-field magnetization as well as neutron scattering and spectroscopic studies are required in order to evaluate the basic magnetic parameters D and J and to resolve the question of the ground state of monoclinic $NiSeO_3$.

Supplementary materials

Supplementary material has been sent to the Fachinformationzentrum Karlsruhe, Abteilung PROKA, 76344 Eggenstein-Leopoldshafen, Germany (fax +49-7247-808-666; e-mail: crysdata@fiz-karlsruhe.de), and can be obtained on quoting the deposit number CSD-416251.

Acknowledgments

This work has in part been carried out with financial support from the Swedish Research Council. The work in Lausanne was supported by the Swiss National Science Foundation (SNSF) and by MaNEP. The work in Zagreb was supported by the resources of the SNSF-SCOPES (Scientific Co-operation between Eastern Europe and Switzerland) project.

References

[1] Johnsson M, Törnroos K W, Lemmens P and Millet P 2003 *Chem. Mater.* **15** 68–73
[2] Johnsson M, Törnroos K W, Mila F and Millet P 2000 *Chem. Mater.* **12** 2853–7
[3] Becker R, Johnsson M, Kremer R K and Lemmens P 2003 *Solid State Sci.* **5** 1411–6
[4] Becker R, Johnsson M, Kremer R K and Lemmens P 2005 *J. Solid State Chem.* **178** 2024–9
[5] Becker R, Berger H, Johnsson M, Prester M, Marhonic Z, Miljak M and Herak M 2006 *J. Solid State Chem.* **179** 836–42
[6] Takagi R, Johnsson M, Gnezdilov V, Kremer R K, Brenig W and Lemmens P 2006 *Phys. Rev.* B **74** 014413
[7] Mayerová Z, Johnsson M and Lidin S 2006 *Angew. Chem. Int. Edn* **45** 5602–6
[8] Kohn K, Inoue K, Horie O and Akimoto S-I 1976 *J. Solid State Chem.* **18** 27–37
[9] Wildner M 1995 *J. Solid State Chem.* **120** 182–6
[10] Effenberger H 1986 *Z. Kristallogr.* **175** 61–72
[11] Wildner M N 1990 *Neues Jahrbuch fuer Mineralogie Monatshefte* **8** 353–62
[12] McManus A V P, Harrison W T A and Cheetham A K 1991 *J. Solid State Chem.* **92** 253–60
[13] Wildner M 1991 *Mon. Chem. verwandte Teile anderer Wiss.* **122** 585–94
[14] Moriya T 1960 *Phys. Rev.* **117** 635–47
[15] Haldane F D M 1983 *Phys. Rev. Lett.* **15** 1153–6
[16] Carlin R L, Joung K O, Filho A P, O'Connor C J and Sinn E 1979 *J. Phys. C: Solid State Phys.* **12** 293–301
[17] Jiang H L and Mao J-G 2006 *Inorg. Chem.* **45** 7593–9

[18] CrysAlis RED 1.171.29.2 Oxford Diffraction, Poland 2006
[19] Sheldrick G-M 1997 *SHELXS-97 Program for the Solution of Crystal Structures* Göttingen
[20] Sheldrick G-M 1997 *SHELXL-97 Program for the Refinement of Crystal Structures* Göttingen
[21] Galy J, Meunier G, Andersson S and Åström E 1975 *J. Solid State Chem.* **13** 142–59
[22] Brown I D and Altermatt D 1985 *Acta Crystallogr.* B **41** 244–7
[23] Liu W and Thorp H H 1993 *Inorg. Chem.* **32** 4102–5
[24] Selwood P W 1956 *Magnetochemistry* 2nd edn (New York: Interscience)
[25] Lines M E 1967 *Phys. Rev.* **164** 736–48
[26] Silverstein S D and Jacobs I S 1964 *Phys. Rev. Lett.* **12** 670–2
[27] Miljak M, Cooper J R and Bechgaard K 1988 *Phys. Rev.* B **37** 4970–4
[28] Dorner B, Visser D, Steigenberger U, Kakurai K and Steiner M 1988 *Z. Phys.* B **72** 487–96
[29] Carlin R L and Van Duyneveldt A J 1977 *Magnetic Properties of Transition Metal Compounds* (New York: Springer)
[30] De Jongh L J and Miedema A R 2001 *Adv. Phys.* **50** 947–1170
De Jongh L J and Miedema A R 2001 *Adv. Phys.* **50** 1076